Nanoscale

Preferred Catalysis Distinctly Determined by Metals Doped with Nitrogen in Three-dimensionally Ordered Porous Carbon Materials

Journal:	*Nanoscale*
Manuscript ID	NR-ART-03-2023-001359.R1
Article Type:	Paper
Date Submitted by the Author:	28-Apr-2023
Complete List of Authors:	Maruyama, Jun; Osaka Research Institute of Industrial Science and Technology, Research Division of Environmental Technology Sato, Hirofumi; Osaka Research Institute of Industrial Science and Technology, Surfactant Lab. Takao, Yuko; Osaka Research Institute of Industrial Science and Technology Maruyama, Shohei; Osaka Research Institute of Industrial Science and Technology, Kato, Shintaro; Osaka University, Engineering science Kamiya, Kazuhide; Osaka University, Chida, Koki; Tohoku University, Yoshii, Takeharu; Tohoku University, Institute of Multidisciplinary Research for Advanced Materials Nishihara, Hirotomo; Tohoku University, Institute of Multidisciplinary Research for Advanced Materials Tani, Fumito; Kyushu University, Institute for Materials Chemistry and Engineering

ARTICLE

Preferred Catalysis Distinctly Determined by Metals Doped with Nitrogen in Three-dimensionally Ordered Porous Carbon Materials

Received 00th January 20xx,
Accepted 00th January 20xx

DOI: 10.1039/x0xx00000x

Jun Maruyama,*[a] Hirohumi Sato,[a] Yuko Takao,[a] Shohei Maruyama,[a] Shintaro Kato,[b] Kazuhide Kamiya,[b] Koki Chida,[c] Takeharu Yoshii,[c] Hirotomo Nishihara,[c,d] Fumito Tani[e]

Three-dimensionally ordered nanoporous structures were generated in carbon materials doped with metals and nitrogen as catalytically active sites for electrochemical reactions. Free-base and metal phthalocyanines with a strategically designed molecular structure were used as carbon sources to attain an ordered porous structure via homogeneous self-assembly with Fe_3O_4 nanoparticles as the pore template and prevention of melting away during carbonization. The doping of Fe and nitrogen was achieved by a reaction between the free-base phthalocyanine and Fe_3O_4 through carbonization at 550 °C, while Co and Ni were doped using the corresponding metal phthalocyanines. The preference of these three types of ordered porous carbon materials for catalytic reactions was distinctly determined by the doped metal. Fe–N-doped carbon showed the highest activity for O_2 reduction. Additional heat treatment at 800 °C enhanced this activity. The CO_2 reduction and H_2 evolution were preferred by the Ni– and Co–N-doped carbon materials, respectively. The change in the template particle size was capable of controlling the pore size to enhance mass transfer and improve performance. The technique presented in this study enabled systematic metal doping and pore size control in the ordered porous structures of carbonaceous catalysts.

Introduction

Porous materials with high specific surface areas have played an important role in chemical industries as adsorbents, catalysts, and catalyst supports.[1–3] Among these materials, those with a three-dimensional (3D) order, such as zeolites,[4,5] mesoporous silica,[6,7] and metal–organic frameworks,[8,9] have gained particular interest. This is because the 3D-ordered pore structure enables maximum surface exposure, efficient mass transfer throughout the pores, and more feasible structure control than disordered ones. The 3D-ordered porosity has also been achieved using carbon materials, which have advantages over other ordered porous materials in terms of electron conductivity and chemical stability.[10,11] Another advantage is the ability to include other elements in the carbon matrix, which imparts various functions.[12,13]

Recently, much attention has been paid to carbon materials containing metal ions coordinated by nitrogen atoms and embedded on the carbon surface (metal–N–C sites) as single-atom catalysts.[14,15] Many studies have shown promising catalytic activities for the oxygen reduction reaction (ORR),[16] oxygen evolution reaction,[17,18] hydrogen evolution reaction (HER),[19,20] CO_2 reduction reaction (CRR),[21] and reduction reactions of nitrogen oxides.[22,23]

In contrast to a large number of studies on 3D-ordered porous carbon materials,[13,24,25] studies on 3D-ordered porous carbon materials compatible with metal–N–C sites are unexpectedly limited, probably because of the difficulties in generating 3D-ordered structures. The formation of carbon materials requires a carbonization process in which polyaromatic ring generation, fusion, and π-conjugation expansion typically occur through random C–C bond formation.[26] In addition, the carbonization process accompanies high temperature, often leading to metal aggregation and, consequently, disordered structures.[27]

One of the approaches to generate 3D-ordered porous carbon (OPC) materials with metal-N-C sites exploited a self-assembled triblock copolymer (Pluronic F127) as a template and phenolic resin as a carbon source.[28,29] Melamine as a nitrogen source was mixed in the resin, and Fe was loaded on the resin with an $FeCl_3$ solution before carbonization. The self-assembly of cubic Fe_3O_4 nanoparticles (NPs) as a template was also used.[30] The carbon materials developed in these studies possessed highly ordered 3D porous structures. However, drawbacks of these approaches were the usage of toxic reagents, such as formaldehyde, to synthesize the phenolic resin or NH_3 to generate micropores and active sites. A recent study avoided the usage of these toxic reagents, although only macropore was 3D-ordered.[31] The

[a] Osaka Research Institute of Industrial Science and Technology, 1-6-50, Morinomiya, Joto-ku, 536-8553 Osaka, Japan
[b] Research Center for Solar Energy Chemistry, Graduate School of Engineering Science, Osaka University, 1-3 Machikaneyama, Toyonaka, Osaka 560-8531, Japan
[c] Institute of Multidisciplinary Research for Advanced Materials, Tohoku University, 2-1-1, Katahira, Aoba-ku, Sendai, 980-8577, Japan
[d] Advanced Institute for Materials Research (WPI-AIMR), Tohoku University, 2-1-1, Katahira, Aoba-ku, Sendai, 980-8577, Japan
[e] Institute for Materials Chemistry and Engineering, Kyushu University, 744, Motooka, Nishi-ku, Fukuoka 819-0395, Japan
Electronic Supplementary Information (ESI) available. See DOI: 10.1039/x0xx00000x

generation of the metal–N–C structure is not fully controlled in these studies, either.

We recently achieved total structure control during carbonization to form 3D-ordered carbon materials with metal–N–C sites.[32,33] The 3D-ordered structure was directly derived from a crystal of a metal porphyrin with alkynyl substituents that underwent polymerization without disorder or destruction of the metal–N–C sites during the carbonization process. However, their limited specific surface areas and pore sizes hinder active site exposure and catalytic electrochemical processes.

Combining the advantages of these techniques, we attempted to form a mesoporous 3D-OPC compatible with metal–N–C sites using a simpler and safer process, based on expectation that he mesoporosity could enhance the active site exposure and fast mass-transfer. A free-base phthalocyanine and metal phthalocyanines (metal = Co, Ni) with octynyl substituents[33–36] were chosen because of the potentially higher rigidity of the metal–N center than porphyrins and their high solubility in organic solvents, which allowed the preparation of a homogeneous mixture with Fe_3O_4 NPs dispersed in toluene. The advantages of using the Fe_3O_4 NPs dispersion are easy availability, small particle sizes down to 5 nm, and self-assemble ability.[37] We found that the Fe_3O_4 NPs functioned as a template for the 3D-ordered structure[38] and as a metal source for the Fe–N–C site, which was included in the carbonaceous phase derived from the octynyl-substituted phthalocyanine. Co– and Ni–N–C sites were also generated using their respective metal phthalocyanines. The electrochemical catalytic activity was closely associated with the metal species, and the pore size was attributed to the NP size. We found another versatile, feasible, and universal approach to synthesize metal–N–C containing 3D-ordered porous carbon materials.

Results and discussion

Synthesis of 3D-OPC

As the sources of the carbonaceous matrix and active sites, the phthalocyanines with the alkynyl substituent, 2,3,9,10,16,17,23,24-octa(1-octynyl)phthalocyanine (Pc'), [2,3,9,10,16,17,23,24-octa(1-octynyl)phthalocyaninyl]cobalt(II) (CoPc'), and [2,3,9,10,16,17,23,24-octa(1-octynyl)phthalocyaninyl]nickel(II) (NiPc'), were synthesized according to the previous report (Fig. S1).[34]

Vacant space in a sheet of carbon paper (CP) composed of graphitized carbon fiber with high electron conductivity and chemical stability was used as a field for the self-assembly of MPc' (M = blank, Co, Ni) and Fe_3O_4 NPs to form binder-free composite carbonaceous electrodes directly after the carbonization and template removal. Fe_3O_4 NPs dispersions in toluene with two different average particle sizes of *m* nm (NP*m*, *m* = 5 and 10) were used as a template for 3D ordered pores.

A piece of CP was immersed in a mixture prepared by dissolving MPc' in NP*m*, which was slowly evaporated to cause the self-assembly in the CP void and completely dried in a vacuum to produce composites (MPc'-NP*m*). Next, the composite was heat-treated in an Ar atmosphere at 550 °C to obtain carbonaceous composites (MPc'-NP*m*-550). The heat-treatment temperature of 550 °C was chosen because it is nearly the upper limit, above which reaction between Fe_3O_4 and carbon becomes thermodynamically favorable, leading to structure disorder. The composite was then treated in a boiling acid solution for template removal, rinsed with high-purity water, and dried in a vacuum to produce the 3D-OPC/CP composites (MPc'-NP*m*-550-a). The carbonaceous composite was also prepared by dissolving MPc' in toluene instead of NP*m*, drying, and the heat-treatment at 550 °C (MPc'-550). The composite obtained after the acid treatment of MPc'-550 is labeled MPc'-550-a. Because electronic conductivity of typical carbon materials enhances with an increase in the carbonization temperature and its drastic increase occurs in the temperature range approximately from 500 to 800 °C,[39,40] the second heat treatment was performed on MPc'-NP*m*-550-a and MPc'-550-a at 800 °C in Ar atmosphere expecting the electronic conductivity improvement. Next, acid treatment yielded MPc'-NP*m*-800-a and MPc'-800-a, respectively. A schematic of the synthesis procedure is shown in Fig. 1, and the series of samples synthesized in this study is summarized in Table 1.

Pyrolysis behavior of MPc'

Thermogravimetry and differential scanning calorimetry (TG–DSC) profiles for MPc' in the He flow are shown in Fig. 2. The significant weight change occurred between 350 and 550 °C and resulted in the weight loss at 550 °C: Pc', 47.7%; CoPc', 34.2%; NiPc', 37.9%. The metal inclusion in Pc' caused the difference in weight loss. The higher and lower ones at the free base Pc' and metal-combined Pc' approximately corresponded to the losses of 8-hexyl and 8-pentyl groups, respectively.

The small peaks around 250 °C in the DSC profiles were attributed to thermal polymerization at the triple bonds.[32,41] After the polymerization, the hexyl and pentyl groups were detached to yield the carbon material. The mass spectrometry (MS) profiles for the effluent gases obtained simultaneously during the TG–DSC measurements also suggested the detachment in the carbonization process of MPc' (Fig. S2).

3D-ordered porous structure

The self-assembly of NP with MPc' in the CP void, the heat treatment in an Ar atmosphere at 550 °C, and the NP removal by the acid treatment produced 3D-OPC. Field-emission scanning electron microscopy (FESEM) images of the 3D-OPC are shown in Fig. 3. Except CoPc'-NP5-550-a, the 3D-ordered porous structure was observed. A Two-dimensional fast Fourier transform (FFT) image[42] indicated a close-packed structure. The homogeneous MPc' distribution in the NP dispersion and the retention of MPc' without melting away during the heat treatment were attributed to the solubility imparted by the hexyl group and the thermal polymerization at the triple bonds, respectively, which led to the 3D ordered pore structure. The external surface of CoPc'-NP5-550-a was covered by the carbonaceous phase, which hindered full exposure of the pore. Observation of the pores was possible irrespective of the M species for MPc'-NP10-550-a. However, the structures were

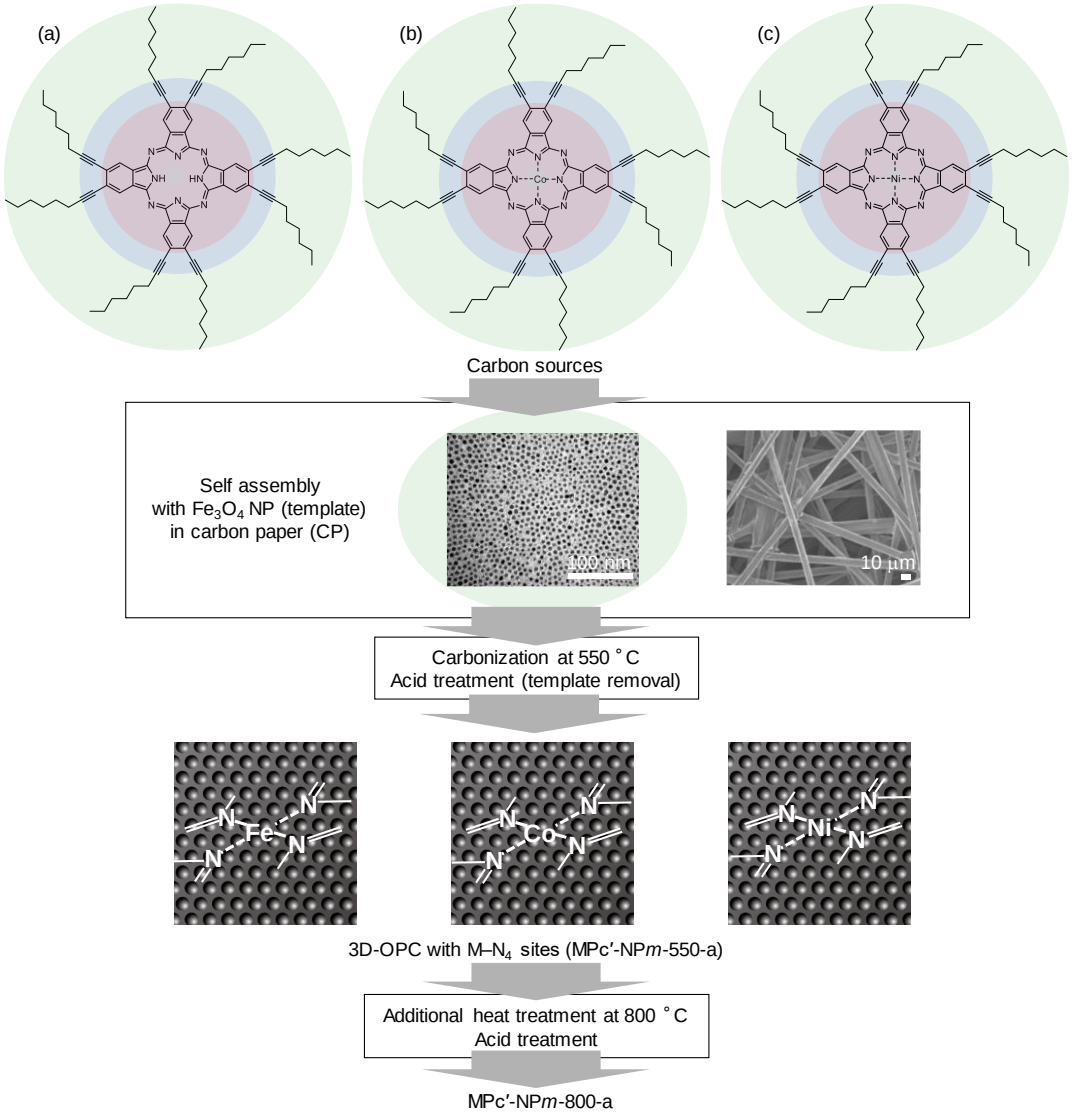

Fig. 1. Synthesis of 3D-OPC/CP composites from octynyl-substituted phthalocyanines: (a) Pc', (b) CoPc', (c) NiPc'. The green, blue, and red parts in the molecular structure show the substructures that enabled the homogeneous self-assembly with the Fe_3O_4 NPs as the pore template and the prevention of melting away during the carbonization process through the polymerization, and the generation of the metal–N_4 structure, respectively.

Table 1. Series of samples synthesized in this study

Phthalocyanine	Pc'	CoPc'	NiPc'
Self-assembly	Pc'-NP5	CoPc'-NP5	NiPc'-NP5
	Pc'-NP10	CoPc'-NP10	NiPc'-NP10
Heat treatment at 550 °C	Pc'-550	CoPc'-550	NiPc'-550
	Pc'-NP5-550	CoPc'-NP5-550	NiPc'-NP5-550
	Pc'-NP10-550	CoPc'-NP10-550	NiPc'-NP10-550
Acid treatment	Pc'-550-a	CoPc'-550-a	NiPc'-550-a
	Pc'-NP5-550-a	CoPc'-NP5-550-a	NiPc'-NP5-550-a
	Pc'-NP10-550-a	CoPc'-NP10-550-a	NiPc'-NP10-550-a
Heat treatment at 800 °C + acid treatment	Pc'-800-a	CoPc'-800-a	NiPc'-800-a
	Pc'-NP5-800-a	CoPc'-NP5-800-a	NiPc'-NP5-800-a
	Pc'-NP10-800-a	CoPc'-NP10-800-a	NiPc'-NP10-800-a

more disordered than those of MPc'-NP5-550-a. This observation was attributed to the wider particle size distribution in the NP10 dispersion and the possible aggregation of the Fe_3O_4 particles. The pore structure was almost retained after the heat treatment at 800 °C and the similar ordered structure was observed for MPc'-NP*m*-800-a (*m* = 5, 10, Figure

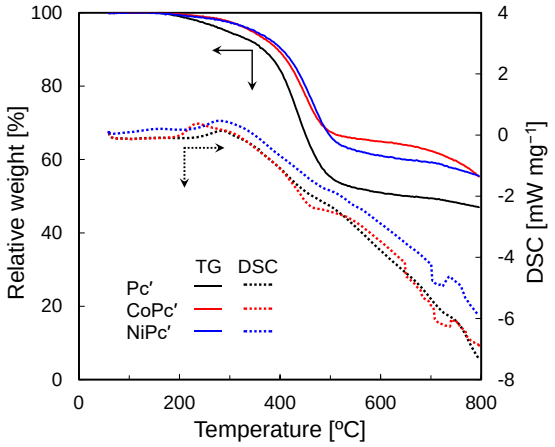

Fig. 2. TG–DSC profiles of Pc′, CoPc′, and NiPc′ under He flow.

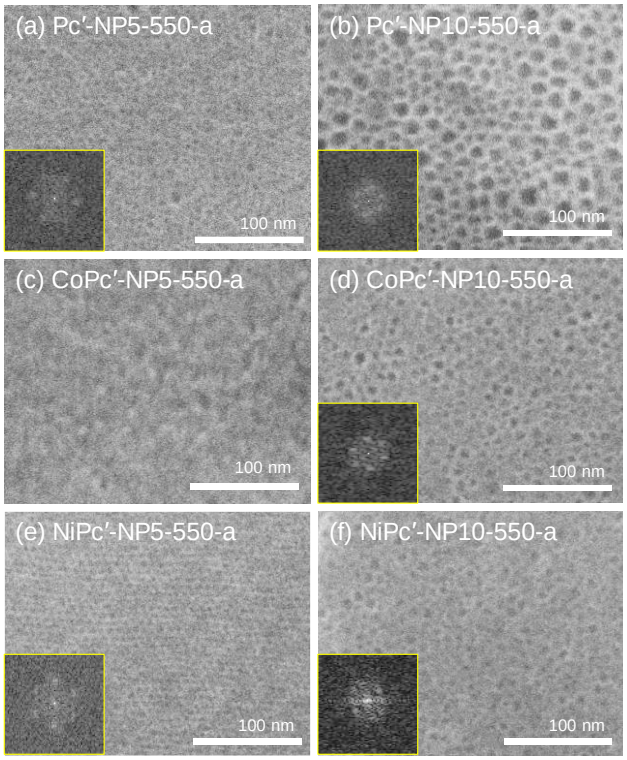

Fig. 3. FESEM images of (a) Pc′-NP5-550-a, (b) Pc′-NP10-550-a, (c) CoPc′-NP5-550-a, (d) CoPc′-NP10-550-a, (e) NiPc′-NP5-550-a, and (f) NiPc′-NP10-550-a. The inset shows the FFT image obtained from the corresponding FESEM image.

S3). Their external surfaces were slightly roughened, probably owing to the partial combustion of the surface by residual oxygen in the atmosphere during heat treatment.

The structure of the carbonaceous pore walls was examined using Raman spectroscopy. Figs. 4 and S4 show the Raman spectra of MPc′-NP*m*-550-a and MPc′-NP*m*-800-a (*m* = 5, 10), respectively. The peak profiles are similar to the typical profiles observed for amorphous carbon materials. The spectra were deconvoluted into five components: graphitic peak (G peak), disorder peak (D peak), a peak ascribed to amorphous carbon (Am peak), a peak ascribed to sp^3-bonded carbon atoms (P peak), and a peak ascribed to the surface graphene layers as a disordered graphitic lattice (D2 peak).[43,44] The ratios of the

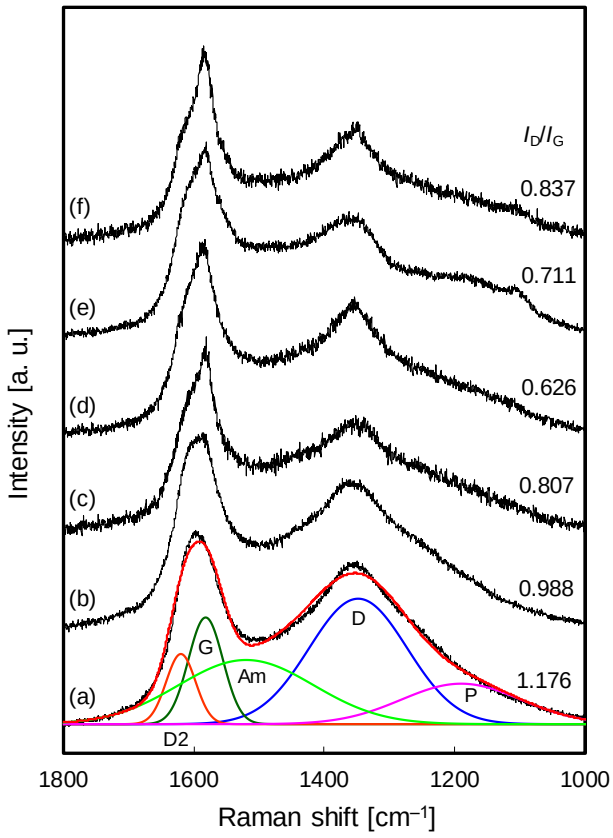

Fig. 4. Raman spectra of (a) Pc′-NP5-550-a, (b) Pc′-NP10-550-a, (c) CoPc′-NP5-550-a, (d) CoPc′-NP10-550-a, (e) NiPc′-NP5-550-a, and (f) NiPc′-NP10-550-a. Deconvoluted components (D2, G, Am, P, D) and fitting result are shown for Pc′-NP5-550-a as a typical example. Values of I_D/I_G are also shown.

intensities of the D peak to the G peak (I_D/I_G) were lower for the spectra of MPc′-derived 3D-OPC (M = Co, Ni) than that of Pc′-derived one, indicating the better crystallinity in the former.

Surface composition of 3D-OPC and local structure around metals

X-ray photoelectron spectroscopy (XPS) was performed to examine the surface elemental composition of 3D-OPC. Fig. 5 shows the XPS spectra of N 1s, Fe 2p, Co 2p, and Ni 2p. The wide scan, C 1s, O 1s, and Cl 2p spectra are presented in Fig. S5 and S6. The atomic surface concentrations of these elements are listed in Table 2.

The N 1s XPS spectra indicated that the nitrogen in MPc′ partly retained in 3D-OPC in the forms of pyridinic, pyrrolic, and graphitic nitrogen atoms[45,46] and that the dominance of the pyridinic nitrogen increased in the order of M: blank < Co < Ni. The Co and Ni 2p spectra also showed retention of the central metals of the phthalocyanines after heat treatment and acid washing.

The most notable result of the XPS measurements was the Fe 2p spectrum, which showed the presence of Fe in Pc′-NP*m*-550-a (*m* = 5, 10). As the sample was obtained after acid treatment, the Fe_3O_4 NPs used as the template were fully removed. The measurements of Fe *K*-edge extended X-ray absorption fine structure (EXAFS) for Pc′-NP*m*-550-a (Fig. 6) showed a pseudoradial structure function (RSF) similar to that of iron

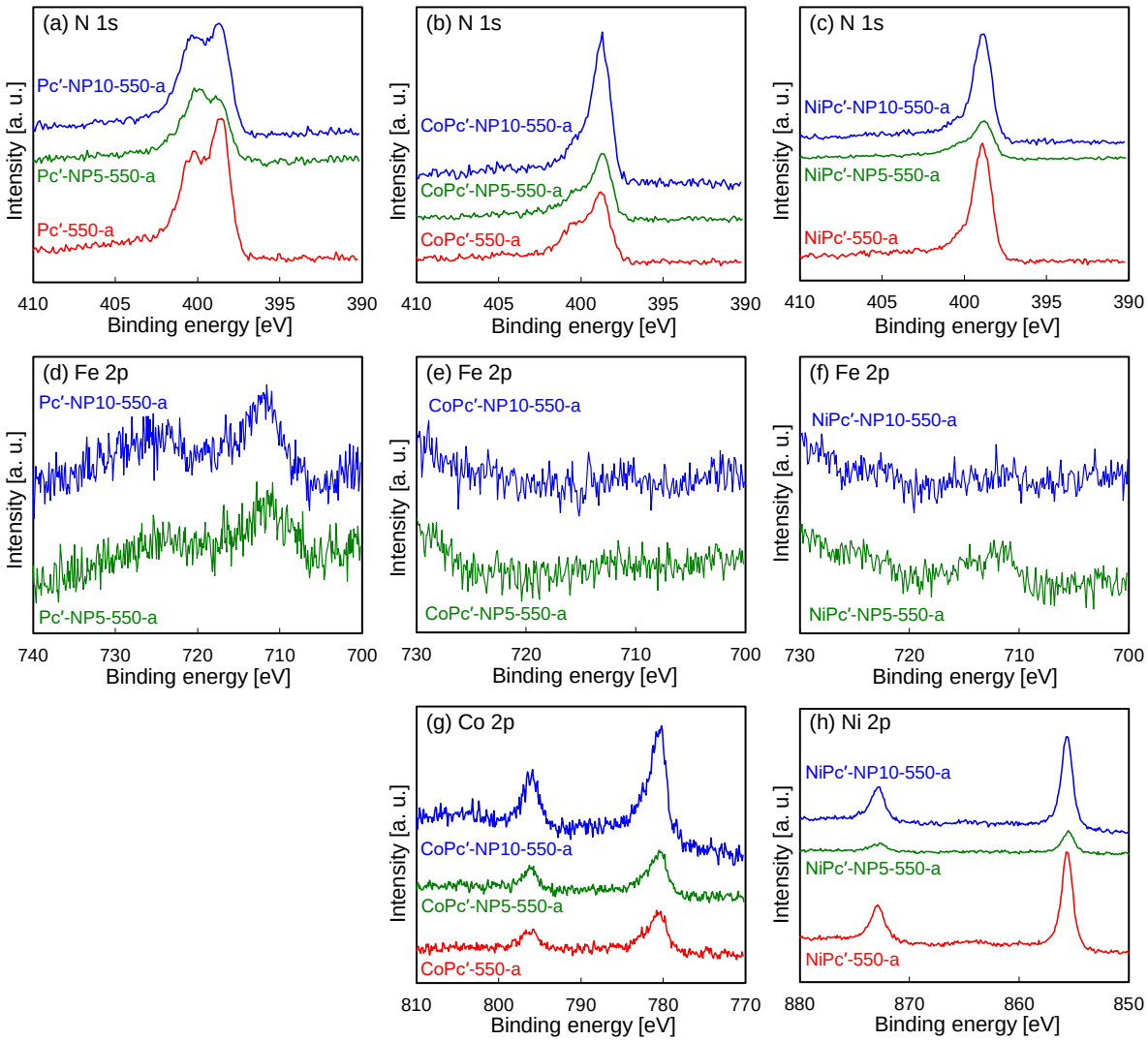

Fig. 5. XPS spectra of (a–c) N 1s, (d–f) Fe 2p, (g) Co 2p, and (h) Ni 2p for MPc′-550-a and MPc′-NP*m*-550-a. The Fe 2p spectra for MPc′-NP*m*-550-a (M = Co, Ni) were obtained by using the Mg Kα radiation. The other spectra were obtained by using the Al Kα radiation. The intensities are normalized by the C 1s peak area of the corresponding samples for easy comparison in each panel.

Table 2. Surface concentrations of MPc′-NP*m*-550-a (*m* = 5, 10) and MPc′-550-a for comparison [atom. %].

	C	N	O	Fe	Co	Ni	Cl
Pc′-550-a	89.08	3.83	6.82	–	–	–	0.17
Pc′-NP5-550-a	86.13	2.32	10.92	0.15	–	–	0.47
Pc′-NP10-550-a	86.95	3.64	8.82	0.16	–	–	0.44
CoPc′-550-a	90.39	2.93	6.22	–	0.16	–	0.30
CoPc′-NP5-550-a	88.21	2.74	8.64	–	0.11	–	0.30
CoPc′-NP10-550-a	88.46	4.51	6.32	–	0.37	–	0.34
NiPc′-550-a	87.71	6.33	5.16	–	–	0.64	0.16
NiPc′-NP5-550-a	88.09	2.60	8.88	0.05	–	0.15	0.23
NiPc′-NP10-550-a	88.09	5.79	5.17	–	–	0.64	0.31

phthalocyanine (FePc), indicating an FePc-like local structure around the Fe atom in Pc′-NP*m*-550-a, that is, four N atoms coordinating Fe in a square-planar structure (Fe–N_4 structure). The absence of the peak attributable to Fe_3O_4 confirmed the full removal of the Fe_3O_4 NPs.

A previous study demonstrated that carbonization of polyaniline surrounding Fe_3O_4 NPs also generated the Fe–N_4 structure.[47] The presence of Fe was therefore attributed to the Fe inclusion in the carbon matrix of 3D-OPC and generation of the Fe–N_4 structure through the reaction between Pc′ and Fe_3O_4

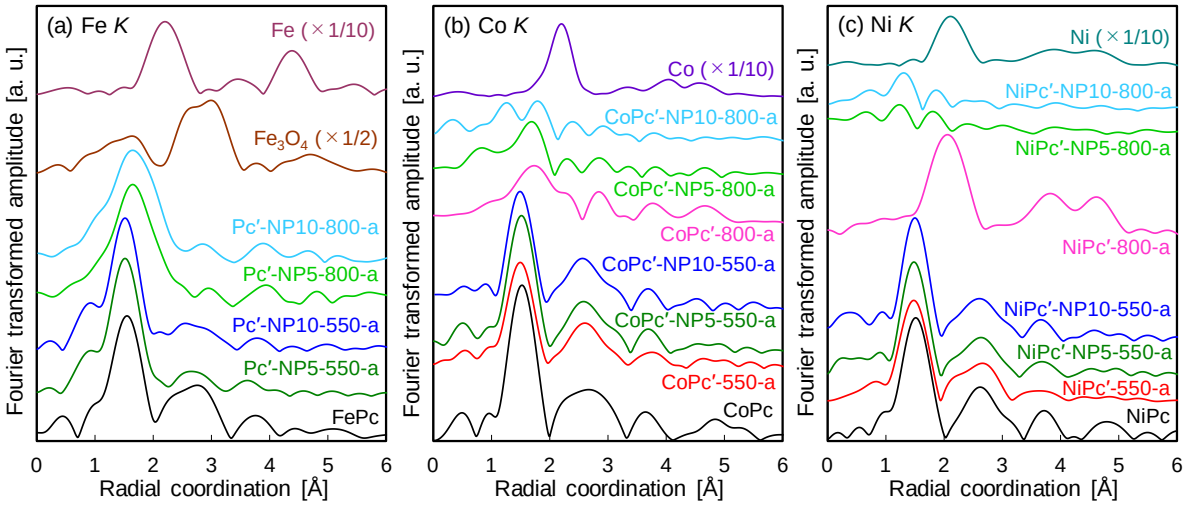

Fig. 6. RSFs calculated by Fourier transformation of EXAFS spectra at the (a) Fe *K*-edge, (b) Co *K*-edge, and (c) Ni *K*-edge for MPc'-*T*-a, MPc'-NP*m*-*T*-a (*m* = 5, 10; *T* = 550, 800), metal foils, metal phthalocyanines, and Fe_3O_4. The amplitudes of the RSFs for the metal foils and Fe_3O_4 are multiplied by 1/10 and 1/2, respectively.

during the heat treatment process and structure retention after the acid treatment.

The Co and Ni *K*-edge EXAFS of MPc'-NP*m*-550-a showed the retention of M–N_4 structure (M = Co, Ni). The presence of Co and Ni was also observed in the XPS spectra. The generation of the Fe–N_4 site was suggested by the RSFs calculated from the Fe *K*-edge EXAFS (Fig. S7), which was ascribed to the reaction between the N atoms or metal substitution in MPc'. However, almost no Fe was observed in the Fe 2p XPS spectra. One of the possible reasons is weaker binding between Fe and N in MPc'-NP*m*-550-a (M = Co, Ni) than in Pc'-NP*m*-550-a, which led to the removal of Fe from the surface by the acid treatment and its retention inside the carbon matrix, although the details are unclear at present.

The surface metals and internal Fe were retained, and more graphitic N was observed after the heat treatment at 800 °C, followed by acid washing (Fig. S7, S8, Table S1). The highest RSF peak for FePc'-NP*m*-800-a was broadened, and the peak position shifted to a larger radial coordination than that of Pc'-NP*m*-550-a. These changes were explained by accounting for the generation of a small peak owing to aggregated Fe and the combination of the peak with that of the Fe–N_4 structure. The aggregated Fe was most likely covered by a carbonaceous shell and retained after the acid treatment.[48] The Fe *K*-edge X-ray absorption near-edge structure (XANES) also showed slight changes (Fig. S9). In contrast to the retention of the Fe–N_4 structure after the 800 °C heat treatment, the loss of the Co– and Ni–N_4 structures was suggested by the RSFs (Fig. 6, Fig. S10) for MPc'-800-a and MPc'-NP*m*-800-a (M = Co, Ni). Except for the RSF for NiPc'-800-a showing the generation of Ni aggregates, there were almost no distinct peaks for the other RSFs, indicating disordered local structures around Co and Ni.

Electrochemical catalytic activity

The relationship between the electrode potential and ORR current in 3D-OPC with the metal–N–C sites is shown in Fig. 7. The peak current increase was observed for Pc'-550-a compared to CP although the positive peak shift was limited, and the reaction faced hindrances in the low potential region, indicating limited activity enhancement by combining the carbonized Pc' with CP (Table S2). In contrast, significant activity enhancement was observed at Pc'-NP5-550-a with a clear peak shift in the positive direction. The Fe–N_4 structure on the 3D-OPC pore surface functioned as active sites for the ORR. The peak current increased at Pc'-NP10-550-a compared to that at Pc'-NP5-550-a, showing the advantageous effect of larger pores for the mass transfer. Additional heat treatment at 800 °C further increased the peak current, probably due to the improved electron conductivity in the carbon matrix, although its activity was lower than that of the Pt/C catalyst.

The catalytic activity of the Co–N_4 structure was implied by the peak shift in the positive direction at CoPc'-550-a compared to Pc'-550-a. This activity was further enhanced at CoPc'-NP5-550-a. The peak potential was slightly lower than that at Pc'-NP5-550-a, whereas a higher peak current was observed. This enhancement was attributed to the pore development and the interaction between the internal Fe–N_4 structure and the Co–N_4 structure on the surface, based on previous studies that showed the ORR activity improvement by the coexistence of the dual metals.[49,50] The effect of the pore size was minor between CoPc'-NP5-550-a and CoPc'-NP10-550-a. The peak current increase by the additional heat treatment at 800 °C was also observed for CoPc'-NP5-800-a. It is reasonable to assume that a Co atom surrounded by N atoms with random bond lengths or a residual Co–N_4 structure functions as the active site for the ORR. The overpotential at a series of 3D-OPCs derived from NiPc' was higher than those derived from Pc' and CoPc', indicating the low ORR activity of the Ni-containing 3D-OPC.

Interestingly, this elemental order for the ORR activity, Fe ≈ Co > Ni, turned opposite for the CRR. Fig. 8 shows the relationship between the electrode potential, CRR/HER current, and current ratio for the CRR/HER. The Pc'-derived 3D-OPC showed limited CRR/HER current with low CRR current efficiency, whereas the CRR current substantially increased at the NiPc'-derived 3D-OPC.[51] Although the largest reduction current was observed at CoPc'-NP10-550-a, the HER dominated, which was in agreement

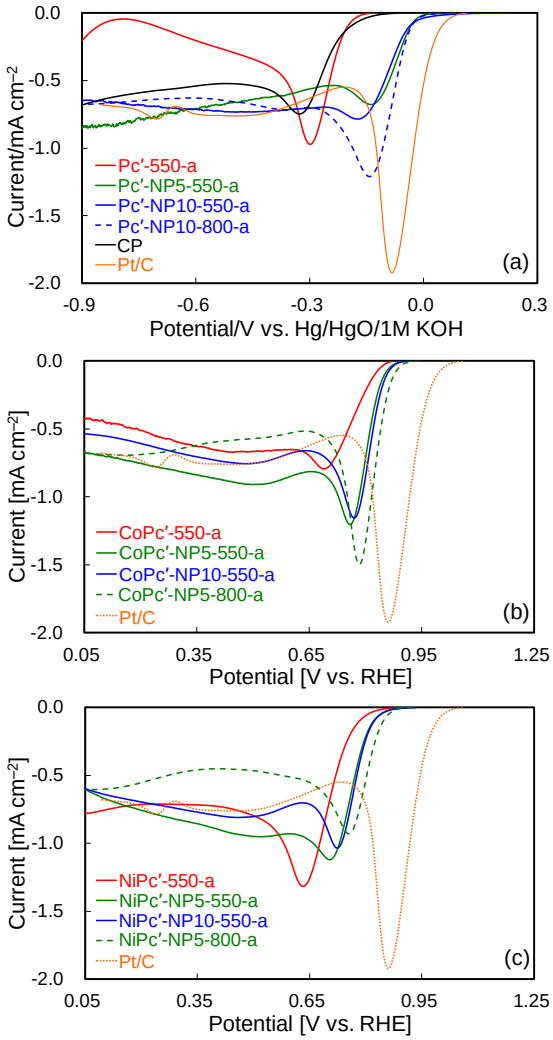

Fig. 7. Relationships between electrode potential and ORR current at MPc′-550-a, MPc′-NP*m*-*T*-a (*m* = 5, 10; *T* = 550, 800) in O_2-saturated 0.1 mol dm^{-3} KOH at 25 °C. The potential scan rate was 10 mV s^{-1}. The relationship at Pt/C is also shown for comparison.

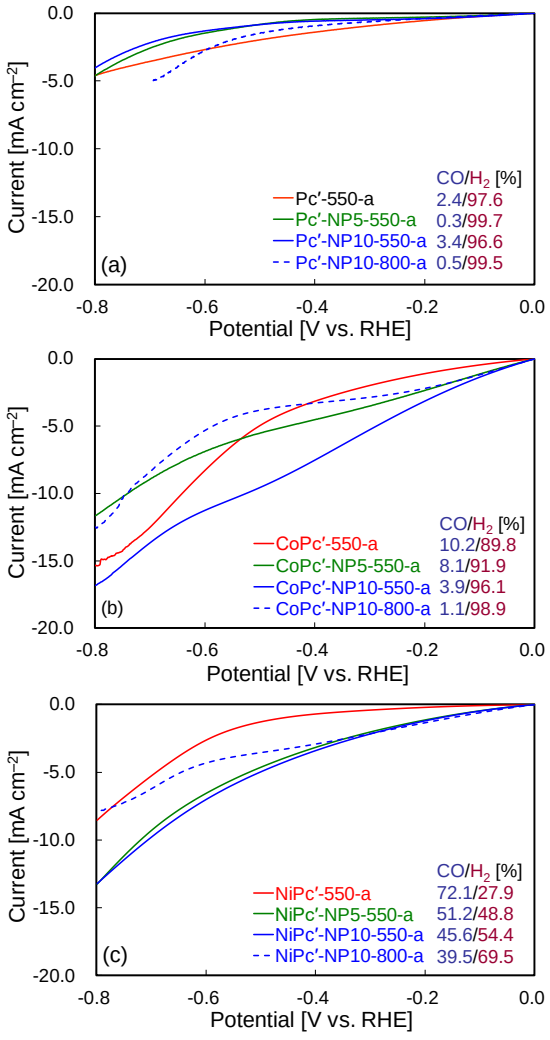

Fig. 8. Relationships between electrode potential and current of CRR and HER at MPc-550-a, MPc′-NP*m*-*T*-a (*m* = 5, 10; *T* = 550, 800) in CO_2-saturated 0.5 mol dm$_{-3}$ $KHCO_3$. The potential scan rate was 10 mV s^{-1}. The ratios of CRR and HER are also shown.

with previous studies showing the high HER activity at Co–N–C catalysts.[52–54] The advantage of the large pore was demonstrated in the CRR/HER at MPc′-NP*m*-550-a (M = Co, Ni) except for the HER in the low potential region at CoPc′-550-a. The slight increase in the current at Pc′-NP10-800-a was also observed, whereas the low current at the 3D-OPC obtained by the additional heat treatment at 800 °C was attributed to the loss of the ordered M–N_4 structure.

Conclusions

The 3D-ordered porous carbon materials, 3D-OPC, with the M-N-C site (M = Fe, Co, Ni) were synthesized from the metal phthalocyanine with the substituent containing the alkyl chain and the triple bond, which enabled the homogeneous self-assembly with the Fe_3O_4 NPs as the pore template and the prevention of melting away during the carbonization process through the polymerization via the triple bond. The Fe–N_4 structure was generated by the reaction between the Fe_3O_4 NPs and the free-base phthalocyanine derivative, while the Co–N_4 and Ni–N_4 structures were imparted to the carbon materials through the retention of the phthalocyanine center of the corresponding metal phthalocyanine derivatives during carbonization. The catalytic activities for ORR, CRR, and HER were heavily dependent on the metal center of the M–N_4 structure on the surface of the 3D-OPCs. The Fe–N–C 3D-OPC was favorable for the ORR but unfavorable for the HER, particularly for the CRR. In contrast, notable CRR activity was only observed for the Ni–N–C 3D-OPC. Co–N–C 3D OPC exhibited moderate activity for the ORR and the highest activity for the HER. Additional heat treatment at 800 °C enhanced the ORR but caused disorder in the Co–N_4 and Ni–N_4 structures. Improved activities for all three reactions were also attained by applying the larger-pore template, which indicated the significance of pore development in 3D OPC, providing an advantage for mass transfer. This study presented a feasible method to synthesize pore-size controlled 3D-OPCs compatible with the metal–N_4 structure. A wide variety of metals could be incorporated as long as the metal-Pc′ is synthesized, potentially leading to catalysts applicable to various reactions.[55,56] The

insufficient catalytic properties in terms of the ORR activity and the CRR selectivity, in particular, are disadvantages to be overcome. One of the promising methods would be usage of a secondary template in addition to the primary Fe_3O_4 NP template, such as 2D-materials[57,58] and nano-size shape ordered metal–organic frameworks,[59–61] to form a nano-size 3D-OPC to further enhance the accessibility to the catalytic active sites.

Experimental

Synthesis of 3D-OPC

The phthalocyanines with the alkynyl substituent, Pc′, CoPc′, and NiPc′, were synthesized according to the previous report.[31] The metal sources were $Co(CH_3CO_2)_2{\cdot}4H_2O$ and $Ni(CH_3CO_2)_2{\cdot}4H_2O$. The generation of Pc′, CoPc′, and NiPc′ was confirmed by matrix-assisted laser desorption/ionization-time of flight (MALDI-TOF)-MS (Bruker Daltonics, AutoFlex II). Fe_3O_4 NPs dispersions in toluene (5 wt.%, including the dispersant) were purchased from Sigma–Aldrich.

A 1 cm^2 piece of CP sheet (TGP-H-090, Toray), with thickness 0.28 mm, and void fraction 0.78 (according to the manufacturer's datasheet) was immersed in a mixture prepared by dissolving 5 mg of MPc′ in 1 cm^3 of NP*m*, which was slowly evaporated to cause the self-assembly in the CP void and completely dried in a vacuum at 90 °C overnight to produce composites (MPc′-NP*m*). Next, the composite was heat-treated in Ar atmosphere at 550 °C for 1h after raising the temperature at a rate of 5 °C min^{-1} to obtain carbonaceous composites (MPc′-NP*m*-550). The composite was then treated in boiling 6 mol dm^{-3} HCl (Nacalai Tesque) for the template removal, rinsed with high-purity water, and dried in a vacuum to produce the 3D-OPC/CP composites (MPc′-NP*m*-550-a). The carbonaceous composite was also prepared by dissolving 5 mg of MPc′ in 1 cm^3 of toluene instead of NP*m*, drying, and the heat treatment at 550 °C (MPc′-550). The composite obtained after the acid treatment of MPc′-550 is labeled MPc′-550-a. Then, the second heat treatment was carried out for MPc′-NP*m*-550-a and MPc′-550-a at 800 °C in an Ar atmosphere for 1h after raising the temperature at a rate of 5 °C min^{-1}, which was followed by the acid treatment to obtain MPc′-NP*m*-800-a and MPc′-800-a, respectively.

Characterization

TG–DSC analysis of MPc′ was performed using a thermogravimeter (STA2500, Netzsch) from 60 to 800 °C at 10 °C min^{-1} under He flow (150 cm^3 min^{-1}). The effluent gas from the TG–DSC measurements was analyzed using a quadrupole mass spectrometer (JMS-Q1500GC, JEOL). FESEM images were obtained using a JSM-6700F (JEOL). FFT images were obtained using ImageJ software.[36] Raman spectra were recorded using a Raman spectrometer (LabRAM HR Evolution, HORIBA) with a 532 nm laser as the excitation source. X-ray photoelectron spectroscopy (XPS) was performed using an AXIS ULTRA DLD system (Kratos Analytical) with Al Kα (1486.6 eV) and Mg Kα (1235.6 eV) radiation. Mg Kα radiation was used to obtain the Fe 2p spectra of MPc′-NP*m*-550-a (M = Co, Ni) to avoid interference from the LMM Auger peaks. The measurements of X-ray absorption fine structures were performed in air at room temperature in fluorescence mode with a 19-element Ge solid-state detector using synchrotron radiation at the BL14B2 beamline of SPring-8 at the Japan Synchrotron Radiation Research Institute. The incident angle of the X-ray beam on the sample surface was approximately 45°, and the detector was directed perpendicular to the beam. The RSF was obtained through Fourier transformation of the k^3-weighted EXAFS spectra using the REX2000 program (Rigaku).

Evaluation of electrochemical catalytic activity

The 3D-OPC/CP composite was fixed on a glassy carbon plate (GC, 10 × 10 × 1 mm, BAS) to form an electrode, and its catalytic activity was evaluated. The GC surface was polished with a 0.05 μm alumina suspension (Baikowski) and ultrasonically cleaned in high-purity water, which was obtained using a Barnstead MicroPure water purification system (Thermo Scientific). The GC surface was then masked using a polytetrafluoroethylene (PTFE) adhesive tape (Nitoflon No. 903UL, Nitto Denko) with an opening of 5 mm × 10 mm. The 3D-OPC/CP composite was cut into pieces of 5 mm × 10 mm, placed on the GC surface, and fixed by covering the upper and lower parts of the composite with a width of 1 mm using a PTFE adhesive tape; only the PTFE side faced the composite and electrolyte. An Au wire was fixed to the back of the GC plate to form a working electrode. In order for the electrolyte to fully penetrate into the pores of the 3D-OPC/CP composite, the working electrode was soaked in boiling high-purity water at a reduced pressure and room temperature (approximately 23 °C) before immersing it in the electrolyte.

A composite of CP and Pt-loaded carbon black (Pt/C, Pt loading of 20 wt.%, Johnson & Matthey) was prepared as a reference for the catalytic activity evaluation. An aliquot of 6.3 mg of Pt/C was added to a 1 cm^3 aqueous solution containing 0.214 cm^3 of 2-propanol (Kanto Chemical) and a 71.6 mm^3 of the 5 wt.% Nafion solution (Sigma–Aldrich) and dispersed ultrasonically. An aliquot of 40 mm^3 of the Pt/C dispersion was immersed in TGP (1 cm^2) and dried to form the Pt/C–CP composite containing 0.25 mg cm^{-2} of Pt/C (Pt, 0.05 mg cm^{-2}).

The electrolyte for evaluating ORR was 0.1 mol dm^{-3} KOH prepared by diluting 3 mol dm^{-3} KOH (Ultrapure, Kanto Chemical) with high-purity water. The counter electrode was a strip of carbon cloth (ElectroChem), and the reference electrode was Hg/HgO/0.1 mol dm^{-3} KOH. The electrode potential was plotted against the reversible hydrogen electrode (RHE). Electrochemical measurements were performed using a three-electrode glass cell and an electrochemical analyzer (ALS760E, BAS). Before the catalytic activity evaluation, the steady-state cyclic voltammogram was obtained in the Ar-saturated electrolyte by repetitive potential scans at 10 mV s^{-1} between 0.05 and 1.25 V. The background current was recorded by the potential scan from 1.25 to 0.05 V at 10 mV s^{-1} and 25 °C. The ORR current was measured after saturation of the electrolyte with oxygen. The ORR current was calculated by subtracting the background current from the measured value.

The catalytic activities for CRR and HER were also evaluated using a 2-compartment cell (VB9B, EC Frontier) and an electrochemical analyzer (HZ-5000, Hokuto Denko). The electrolyte, 0.5 mol dm^{-3} $KHCO_3$ saturated with CO_2, was placed in the working electrode compartment. Ag/AgCl/saturated KCl was used as the reference electrode. The electrode potential was plotted against the RHE. The counter electrode was a Pt wire placed in the other compartment, separated by a Nafion N117 (Chemours) membrane. The membrane was successively immersed in 3% H_2O_2, high-purity water, 1 mol dm^{-3} H_2SO_4, and high-purity water at boiling temperatures before use. The current–voltage curve was measured by the negative potential scan from at 10 mV s^{-1}. The current efficiency was obtained by analyzing the gas accumulated above the electrolyte during electrolysis at −0.8 V up to 1.5 C with a gas chromatograph–mass spectrometer (GCMS-QP 2010 Plus, Shimadzu).

Author Contributions

J. M. designed the experiments, performed the carbonization and electrochemical measurements, interpreted the experimental results, and wrote the manuscript with input from all authors. H. S., Y. T., and F. T. provided information on phthalocyanine synthesis, synthesized the phthalocyanines, and analyzed the products. S. M., K. C., T. Y., and H. N. characterized the carbonization process and the carbon materials. S. K. and K. K. performed the electrochemical measurements.

Conflicts of interest

There are no conflicts to declare.

Acknowledgements

This study was supported by Grants-In-Aid for Scientific Research (KAKENHI; grant nos. 18K04870 and 21K05239) from the Japan Society for the Promotion of Science, Network Joint Research Center for Materials and Devices (no. 20224011), and JST CREST (grant no. JPMJCR18R3). The XAFS measurements were performed with the approval of SPring-8 (Proposal No. 2020A1604). We thank Dr. T. Shinagawa for drawing a part of the schematic.

Notes and references

1 J. Zhang and C. M. Li, *Chem. Soc. Rev.*, 2012, **41**, 7016.
2 B. Fang, J. H. Kim, M. -S. Kim and J. -S. Yu, *Acc. Chem. Res.*, 2013, **46**, 1397.
3 M. -H. Sun, S. -Z. Huang, L. -H. Chen, Y. Li, X. -Y. Yang, Z. -Y. Yuan and B. -L. Su, *Chem. Soc. Rev.*, 2016, **45**, 3479.
4 Y. Chai, W. Dai, G. Wu, N. Guan and L. Li, *Acc. Chem. Res.*, 2021, **54**, 2894.
5 T. Weissenberger, A. G. F. Machoke, B. Reiprich and W. Schwieger, *Adv. Mater. Interfaces*, 2021, **8**, 2001653.
6 F. Olivieri, R. Castaldo, M. Cocca, G. Gentile and M. Lavorgna, *Nanoscale*, 2021, **13**, 9091.
7 H. Li, X. Chen, D. Shen, F. Wu, R. Pleixats and J. Pan, *Nanoscale*, 2021, **13**, 15998.
8 S. Horike, S. S. Nagarkar, T. Ogawa and S. Kitagawa, *Angew. Chem. Int. Ed.*, 2020, **59**, 6652.
9 N. Hosono and S. Kitagawa, *Acc. Chem. Res.*, 2018, **51**, 2437.
10 A. -H. Lu and F. Schüth, *Adv. Mater.*, 2006, **18**, 1793.
11 H. Nishihara and T. Kyotani, *Adv. Mater.*, 2012, **24**, 4473.
12 C. Zhu, H. Li, S. Fu, D. Du and Y. Lin, *Chem. Soc. Rev.*, 2016, **45**, 517.
13 M. R. Benzigar, S. N. Talapaneni, S. Joseph, K. Ramadass, G. Singh, J. Scaranto, U. Ravon, K. Al-Bahily and A. Vinu, *Chem. Soc. Rev.*, 2018, **47**, 2680.
14 M. Shao, Q. Chang, J. -P. Dodelet and R. Chenitz, *Chem. Rev.*, 2016, **116**, 3594.
15 B. Singh, V. Sharma, R. P. Gaikwad, P. Fornasiero, R. Zbořil and M. B. Gawande, *Small*, 2021, **17**, 2006473.
16 Y. He, S. Liu, C. Priest, Q. Shi and G. Wu, *Chem. Soc. Rev.*, 2020, **49**, 3484.
17 H. Fei, J. Dong, Y. Feng, C. S. Allen, C. Wan, B. Volosskiy, M. Li, Z. Zhao, Y. Wang, H. Sun, P. An, W. Chen, Z. Guo, C. Lee, D. Chen, I. Shakir, M. Liu, T. Hu, Y. Li, A. I. Kirkland, X. Duan and Y. Huang, *Nat. Cat.*, 2018, **1**, 63.
18 J. Maruyama, S. Maruyama, T. Fukuhara, H. Mizuhata, S. Takenaka, A. Yoshida and K. Miyazaki, *J. Electrochem. Soc.*, 2020, **167**, 060504.
19 J. Maruyama, T. Ioroi, T. Hasegawa, T. Mori, Y. Orikasa and Y. Uchimoto, *ChemCatChem*, 2014, **6**, 2197.
20 H. Fei, J. Dong, M. J. Arellano-Jiménez, G. Ye, N. D. Kim, E. L. G. Samuel, Z. Peng, Z. Zhu, F. Qin, J. Bao, M. J. Yacaman, P. M. Ajayan, D. Chen and J. M. Tour, *Nat. Commun.*, 2015, **6**, 8668.
21 H. Choi, D. -K. Lee, M. -K. Han, G. Janani, S. Surendran, J. H. Kim, J. K. Kim, H. Cho and U. Sim, *J. Electrochem. Soc.*, 2020, **167**, 164503.
22 D. H. Kim, S. Ringe, H. Kim, S. Kim, B. Kim, G. Bae, H. -S. Oh, F. Jaouen, W. Kim, H. Kim and C. H. Choi, *Nat. Commun.*, 2021, **12**, 1856.
23 Z. -Y. Wu, M. Karamad, X. Yong, Q. Huang, D. A. Cullen, P. Zhu, C. Xia, Q. Xiao, M. Shakouri, F. -Y. Chen, J. Y. Kim, Y. Xia, K. Heck, Y. Hu, M. S. Wong, Q. Li, I. Gates, S. Siahrostami and H. Wang. *Nat. Commun.*, **2021**, *12*, 2870.
24 H. Nishihara and T. Kyotani, *Adv. Mater.*, 2012, **24**, 4473.
25 B. Szczęśniak, J. Choma and M. Jaroniec, *Chem. Commun.*, 2020, **56**, 7836.
26 J. Maruyama, J. Okamura, K. Miyazaki, Y. Uchimoto and I. Abe, *J. Phys. Chem. C*, 2008, **112**, 2784.
27 G. Faubert, G. Lalande, R. Côté, D. Guay, J. P. Dodelet, L. T. Weng, P. Bertrand and G. Dénès, *Electrochim. Acta*, 1996, **41**, 1689.
28 H. Tana, Y. Lia, X. Jiang, J. Tang, Z. Wang, H. Qian, P. Mei, V. Malgras, Y. Bando and Y. Yamauchi, *Nano Energy*, 2017, **36**, 286.
29 S. H. Lee, J. Kim, D. Y. Chung, J. M. Yoo, H. S. Lee, M. J. Kim, B. S. Mun, S. G. Kwon, Y. -E. Sung and T. Hyeon, *J. Am. Chem. Soc.*, 2019, **141**, 2035.
30 B. Wang, X. Wang, J. Zou, Y. Yan, S. Xie, G. Hu, Y. Li and A. Dong, *Nano Lett.*, 2017, **17**, 2003.
31 Z. Zhu, H. Yin, Y. Wang, C. -H. Chuang, L. Xing, M. Dong, Y. -R. Lu, G. Casillas-Garcia, Y. Zheng, S. Chen, Y. Dou, P. Liu, Q. Cheng and H. Zhao, *Adv. Mater.*, 2020, **32**, 2004670.
32 H. Nishihara, T. Hirota, K. Matsuura, M. Ohwada, N. Hoshino, T. Akutagawa, T. Higuchi, H. Jinnai, Y. Koseki, H. Kasai, Y. Matsuo, J. Maruyama, Y. Hayasaka, H. Konaka, Y. Yamada, S. Yamaguchi, K. Kamiya, T. Kamimura, H. Nobukuni and F. Tani, *Nat. Commun.*, 2017, **8**, 109.
33 K. Chida, T. Yoshii, M. Ohwada, Y. Hayasaka, J. Komeda, R. Sakamoto, J. Maruyama, K. Kamiya, M. Inoue, F. Tani and H. Nishihara, *Catal. Today*, 2023, **411-412**, 113830.
34 D. S. Terekhov, K. J. M. Nolan, C. R. McArthur and C. C. Leznoff, *J. Org. Chem.*, 1996, **61**, 3034.
35 R. Faust, *Eur. J. Org. Chem.*, 2001, **2001**, 2797.

36 G. Bottari, D. D. Díaz and T. Torres, *J. Porphyr. Phthalocyanines*, 2006, **10**, 1083.
37 G. Singh, H. Chan, A. Baskin, E. Gelman, N. Repnin, P. Král, R. Klajn, *Science*, 2014, **345**, 1149.
38 J. Maruyama, S. Maruyama, Y. Kashiwagi, M. Watanabe, T. Shinagawa, T. Nagaoka, T. Tamai, N. Ryu, K. Matsuo, M. Ohwada, K. Chida, T. Yoshii, H. Nishihara, F. Tani and H. Uyama, *Nanoscale*, 2022, **14**, 3748.
39 A. Kostuch, S. Jarczewski, M. K. Surówka, P. Kuśtrowski, Z. Sojka and K. Kruczała, *Catal. Sci. Technol.*, 2021, **11**, 7578.
40 Y. -R. Rhim, D. Zhang, D. H. Fairbrother, K. A. Wepasnick, K. J. Livi, R. J. Bodnar, D. C. Nagle, *Carbon*, 2010, **48**, 1012.
41 T. Ogoshi, Y. Sakatsume, K. Onishi, R. Tang, K. Takahashi, H. Nishihara, Y. Nishina, B. D. L. Campéon, T. Kakuta and T. Yamagishi, *Commun. Chem.*, 2021, **4**, 75.
42 C. A. Schneider, W. S. Rasband and K. W. Eliceiri, *Nat. Methods*, 2012, **9**, 671.
43 A. Sadezky, H. Muckenhuber, H. Grothe, R. Niessner and U. Pöschl, *Carbon*, 2005, **43**, 1731.
44 F. Jaouen, F. Charreteur and J. P. Dodelet, *J. Electrochem. Soc.*, 2006, **153**, A689.
45 J. M. Jiménez Mateos and J. L. G. Fierro, *Surf. Interface Anal.*, 1996, **24**, 223.
46 J. Casanovas, J. M. Ricart, J. Rubio, F. Illas and J. M. Jiménez-Mateos, *J. Am. Chem. Soc.*, 1996, **118**, 8071.
47 R. Venegas, C. Zúñiga, J. H. Zagal, A. Toro-Labbé, J. F. Marco, N. Menéndez, K. Muñoz-Becerra and F. J. Recio, *ChemElectroChem*, 2022, **9**, e202200115.
48 J. Maruyama, S. Maruyama, H. Mizuhata, S. Takenaka and A. Yoshida, *J. Electrochem. Soc.*, 2020, **167**, 160520.
49 J. Maruyama, T. Shinagawa, Z. Siroma and A. Mineshige, *Tanso* 2014, **2014**, 165.
50 G. Chen, H. Zhong and X. Feng, *Chem. Sci.*, 2021, **12**, 15802.
51 P. Su, K. Iwase, S. Nakanishi, K. Hashimoto and K. Kamiya, *Small*, 2016, **12**, 6083.
52 J. Maruyama, T. Ioroi, Z. Siroma, T. Hasegawa and A. Mineshige, *ChemCatChem*, 2013, **5**, 130.
53 J. Maruyama, T. Ioroi, T. Hasegawa, T. Mori, Y. Orikasa, and Y. Uchimoto, *ChemCatChem* 2014, **6**, 2197.
54 H. Fei, J. Dong, M. J. Arellano-Jiménez, G. Ye, N. D. Kim, E. L. G. Samuel, Z. Peng, Z. Zhu, F. Qin, J. Bao, M. J. Yacaman, P. M. Ajayan, D. Chen and J. M. Tour, *Nat. Commun.*, 2015, **6**, 8668.
55 J. Maruyama, T. Hasegawa, S. Iwasaki, T. Fukuhara, Y. Orikasa and Y. Uchimoto, *ChemCatChem*, 2015, **7**, 2305.
56 M. Xia, H. Huang, X. Zhang, Q. -H. Wei and Z. Xie, *Phys. Chem. Chem. Phys.*, 2021, **23**, 14276.
57 B. Huang, Y. Liu and Z. Xie, *J. Energy Chem.*, 2021, **54**, 795.
58 Y. Liu, B. Huang, X. Zhang, X. Huang and Z. Xie, *J. Power Sources*, 2019, **412**, 125.
59 G. Zhang, Y. Li, X. Xiao, Y. Shan, Y. Bai, H. -G. Xue, H. Pang, Z. Tian and Q. Xu, *Nano Lett.*, 2021, **21**, 3016.
60 W. Li, X. Guo, P. Geng, M. Du, Q. Jing, X. Chen, G. Zhang, H. Li, Q. Xu, P. Braunstein and H. Pang, *Adv. Mater.*, 2021, **33**, 2105163.
61 S. Zheng, Y. Sun, H. Xue, P. Braunstein, W. Huang and H. Pang, *Natl. Sci. Rev.*, 2022, **9**, nwab197.